AN ASSESSMENT OF MAGNETIC CONDITIONS FOR STRONG CORONAL HEATING IN SOLAR ACTIVE REGIONS BY COMPARING OBSERVED LOOPS WITH COMPUTED POTENTIAL FIELD LINES

D. A. FALCONER[1]

University of Alabama, Huntsville

AND

G. A. GARY, R. L. MOORE, AND J. G. PORTER

Marshall Space Flight Center/NASA, ES82, Huntsville, AL 35812

ABSTRACT

We report further results on the magnetic origins of coronal heating found from registering coronal images with photospheric vector magnetograms. For two complementary active regions, we use computed potential field lines to examine the global nonpotentiality of bright extended coronal loops and the three-dimensional structure of the magnetic field at their feet, and assess the role of these magnetic conditions in the strong coronal heating in these loops. The two active regions are complementary, in that one is globally potential and the other is globally nonpotential, while each is predominantly bipolar, and each has an island of included polarity in its trailing polarity domain. We find the following: (1) The brightest main-arch loops of the globally potential active region are brighter than the brightest main-arch loops of the globally strongly nonpotential active region. (2) In each active region, only a few of the main-arch magnetic loops are strongly heated, and these are all rooted near the island. (3) The end of each main-arch bright loop apparently bifurcates above the island, so that it embraces the island and the magnetic null above the island. (4) At any one time, there are other main-arch magnetic loops that embrace the island in the same manner as do the bright loops but that are not selected for strong coronal heating. (5) There is continual microflaring in sheared core fields around the island, but the main-arch bright loops show little response to these microflares.

From these observational and modeling results we draw the following conclusions: (1) The heating of the main-arch bright loops arises mainly from conditions at the island end of these loops and not from their global nonpotentiality. (2) There is, at most, only a loose coupling between the coronal heating in the bright loops of the main arch and the coronal heating in the sheared core fields at their feet, although in both the heating is driven by conditions/events in and around the island. (3) The main-arch bright loops are likely to be heated via reconnection driven at the magnetic null over the island. The details of how and where (along the null line) the reconnection is driven determine which of the split-end loops are selected for strong heating. (4) The null does not appear to be directly involved in the heating of the sheared core fields or in the heating of an extended loop rooted in the island. Rather, these all appear to be heated by microflares in the sheared core field.

Subject headings: Sun: corona — Sun: magnetic fields — Sun: X-rays, gamma rays

1. INTRODUCTION

The heating of the solar corona remains a major mystery of solar physics, of broad importance to astrophysics in general and to space physics in particular. The coronal X-ray images from *Skylab* dramatically showed that the corona is full of X-ray–emitting plasma that is strongly and intricately sculpted by the magnetic fields permeating it. These images, in combination with photospheric magnetograms, showed that the X-ray brightness of the corona is strongly modulated by the magnetic field, being brighter wherever magnetic field is concentrated, most noticeably in active regions and their miniature counterparts, ephemeral regions (coronal bright points). The same rule applies to all of the magnetically closed corona (everywhere outside of coronal holes) on scales larger than active regions: the brighter the X-ray corona, the stronger the magnetic field in which it resides. By showing that nearly all coronal heating is directly tied to the magnetic field—indicating that if the

Sun had no magnetic field, it would have little or no X-ray corona and little or no solar wind—the coronal images from *Skylab* established that the Sun's coronal heating is largely a consequence of the magnetic field (e.g., Vaiana & Rosner 1978). Beyond this key advance of finding that the magnetic field is inherent in the heating, there has been little further progress in determining the coronal heating process; how the heating results from the magnetic field remains obscure.

Our approach to probing the magnetic origins of coronal heating has been to examine the magnetic structure of sites of strong coronal heating in active regions (Moore et al. 1994; Porter et al. 1994; Falconer et al. 1997; Porter, Falconer, & Moore 1998). Active regions with major sunspots are the largest concentrations of strong magnetic field found on the Sun and display the strongest quasi-steady coronal heating (brightest nonflare coronal X-ray features). Hence, if coronal heating is linked to the structure or configuration of the magnetic field, this linkage might be more obvious in active regions than elsewhere on the Sun.

Our main previous study of coronal heating in active regions is Falconer et al. (1997), which showed that the

[1] Marshall Space Flight Center/NASA, SD50 Huntsville, AL 35812; david.falconer@msfc.nasa.gov.

coronal heating in active regions indeed depends not only on the strength of the magnetic field but on the local structure of the field as well. The results of that study come from the registration of persistent-brightness coronal X-ray images of active regions with maps of neutral-line magnetic shear in those active regions. Examples of such composite images for two representative active regions are reproduced in Figures 1 and 2. Each persistent-brightness image is constructed from a sequence of *Yohkoh* Soft X-Ray Telescope (SXT) coronal images distributed over an orbit. The brightness of each pixel of the persistent-brightness image is the minimum brightness of that pixel in the sequence. With a brightness threshold of 1000 DN s^{-1} pixel^{-1}, such an extracted image shows only those coronal features that were persistently bright (thus strongly heated) through the entire observing interval of the orbit. A neutral-line magnetic shear map of the active region is constructed from the Marshall Space Flight Center (MSFC) vector magnetogram and shows the location of the neutral lines with strong transverse fields ($\gtrsim 150$ G), as well as the degree of shear (the angle between the observed and potential tranverse field) along the neutral line.

From an extensive sample of persistently bright coronal features in active regions, Falconer et al. (1997) found that all such bright features were rooted in strong magnetic field (>150 G) and that nearly all could be interpreted as a magnetic loop or cluster of loops that had at least one end rooted near a neutral line in the manner of all the bright features in Figures 1 and 2. They also found that the members of this nearly all-inclusive class of bright features come in two basic varieties: core features and extended loops. A core feature is entirely embedded in the core magnetic field low along a neutral line, whereas an extended loop arches well away from the core fields that are near one end or both ends. All of the labeled bright features in Figures 1 and 2 are extended loops. Some other bright structures in Figure 2 are core features. We assume that both the extended loops and the core-field bright structures in our two active regions are composed of bundles of roughly parallel adjacent magnetic loops that have somewhat different length and brightness and that are not well resolved in the *Yohkoh* X-rays images. The *Transition Region and Coronal Explorer* (*TRACE*) has shown that the coronal loops in active regions have many brightness striations that are too narrow to be resolved by the *Yohkoh* SXT (e.g., Schrijver et al. 1999).

The key result from Falconer et al. (1997) is that the great majority of the persistently bright coronal features were rooted in or near strongly sheared core field, i.e., near intervals of strong neutral-line magnetic shear (shear angle $>45°$). All of the persistently bright coronal features in Figures 1 and 2 are so rooted. Thus, they found that in many active regions strongly sheared core fields are apparently the source of most of the stronger persistent coronal heating.

Falconer et al. (1997) concentrated on the connection of strong coronal heating with the nonpotentiality near the footpoints of loops, but ignored nonpotentiality on scales of
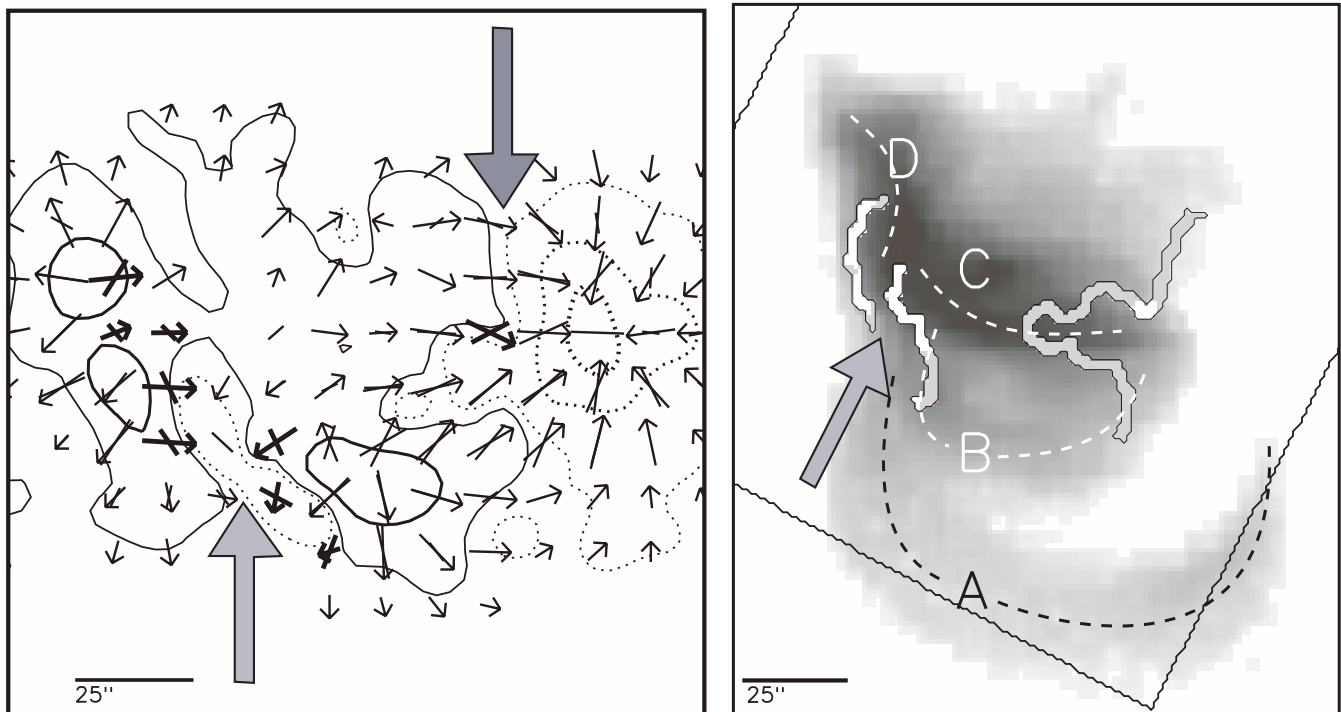

FIG. 1.—Magnetic location of strong coronal heating in an active region that shows little global nonpotentiality (after Fig. 7 of Falconer et al. (1997)). *Left*: MSFC vector magnetogram and superposed computed potential transverse field map (*arrows*). Here and in Fig. 2, for ease of comparing the observed and potential transverse vectors, the vectors are displayed for only every fourth pixel in each direction. *Right*: Persistent-brightness coronal X-ray image superposed on the neutral-line magnetic shear map derived from the vector magnetogram. The tilted square is the field of view of the left panel. The magnetic shear is stronger (shear angle $>45°$) in the white segments and weaker (shear angle $<45°$) in the gray segments. Each of the four features labeled by a letter is a strongly heated extended loop (or cluster of loops) that stems from near the magnetic island with strongly sheared field on its surrounding neutral line. The dimmest of these loops, loop A, has a brightness of about 1000 DN s^{-1} pixel^{-1}. The dashed curve in each of the labeled loop clusters has been drawn by eye, and represents a field line in the center of the loop cluster. The large arrows point out the magnetic island and the main neutral line. In the magnetogram, the transverse field vectors are drawn thick where the shear angle is greater than 45°. This active region is AR 7315 at N5°, E25° on 1992 October 19. Orbit sunrise for the coronal image was at 17:25 UT. The time of the magnetogram is 14:58 UT.
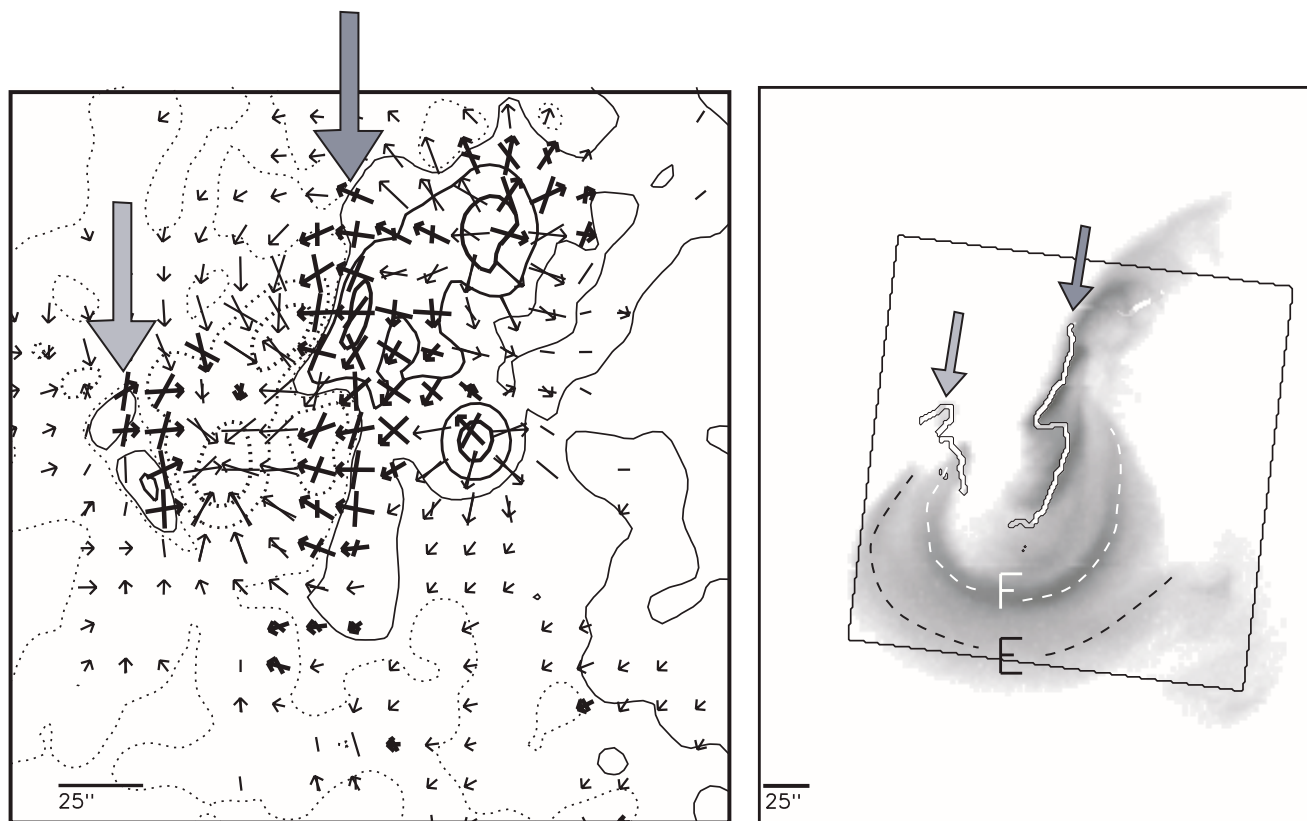
FIG. 2.—Magnetic location of strong coronal heating in an active region that has a magnetic field configuration similar to that of the active region in Fig. 1, but with apparently much greater global nonpotentiality (after Figure 4 of Falconer et al. (1997)). The layout is the same as for Fig. 1. Extended loop C in the other active region is obviously brighter than extended loops E and F in this active region (the brightness is about 10,000 DN s^{-1} pixel^{-1} at the top of loop C and about 5000 DN s^{-1} pixel^{-1} at the top of loop F). In addition to the bright extended loops E and F, the X-ray image shows equally obvious coronal features rooted in the sheared core fields encasing the main neutral line of the active region. This active region is AR 6982 at S10°, W20° on 1991 December 26. Orbit sunrise of the coronal image was at 17:58 UT. The time of the magnetogram is 18:23 UT.

the order of the entire active region. We shall call the non-potentiality on these larger scales *global nonpotentiality*. The term can be ascribed to either single long loops or entire active regions. Loops having little global non-potentiality closely follow the trajectories of potential field lines starting from the same footpoints, whereas the trajec-tories of loops having large global nonpotentiality deviate greatly from the potential field lines rooted at their feet. In the present paper, we investigate whether some of the strong coronal heating in active regions might be more directly tied to the global nonpotentiality of the active region than to the core-field nonpotentiality measured by the neutral-line magnetic shear. Because core features are confined to core fields, it seems likely that the heating of these features depends more on the local core nonpotentiality than on the global nonpotentiality of the overall magnetic envelope, which is rooted mostly well outside of the core fields. In contrast, extended loops are not so confined and are often parts of the overall bipolar envelope of the active region (see Figs. 1 and 2). Thus, it seems possible that the strong coronal heating in extended loops might be more a conse-quence of the global nonpotentiality of these loops than of the core-field nonpotentiality at their feet. Moreover, Fal-coner et al. (1997) found that while a great majority of both core features and extended loops were rooted in strongly nonpotential core fields, this majority for the extended loops was smaller than for the core features: 75% of the extended loops were rooted in or near strongly sheared core

fields, whereas 90% or more of the core features were in such highly nonpotential core fields. This further suggests that the heating in the extended loops might be more directly affected by some other aspect of the field structure, such as the global nonpotentiality of these loops, than by the core-field nonpotentiality near the loop feet. In this paper, we present evidence against this possibility and in favor of neutral-line magnetic shear (core-field nonpotentiality) near the foot of an extended loop being a stronger cause of the enhanced heating in the loop than is the global nonpotentiality of the loop.

In each of our two active regions, most of the extended bright loops are members of the magnetic arch of the overall bipole and stem from around an island of opposite-polarity magnetic flux. (We will refer to the magnetic arch of the overall bipole as the main arch or envelope arch of the active region. Any magnetic flux tube that bridges the neutral line of the overall bipole, i.e., bridges the main neutral line of the active region, and has both feet well away from this neutral line, is a member of the main arch, and is appropriately called a main-arch loop. Many main-arch loops are not bright. Conversely, some bright extended loops are not main-arch loops. An example is the bright loop [or loop cluster] that is rooted near the main neutral line in our second active region and extends out to the northeast [Fig. 2]. In this paper we focus on the bright coronal features rooted in or around the magnetic islands in our two active regions. Many of these features are main-

arch loops, many are core features, and one, loop D [Fig. 1], is an extended loop that is not a main-arch loop.) It is not clear from just the superposition of the X-ray loops on the magnetograms, as in Figures 1 and 2, whether the main-arch bright loops are rooted to one side of the island or have split ends that straddle the island. We use the computed three-dimensional potential field to examine the rooting of these extended loops in the globally nearly potential active region, and find, from the fit of the potential field lines to the observed bright loops of the overall arch, that the ends of these loops probably embrace the magnetic island as sketched in Figure 3: the end of each loop is bifurcated, so that it straddles the magnetic null over the island and the separatrix enclosing the island. This result favors the possibility that these extended loops are heated via reconnection driven at the null by some action of the sheared core field under the dome of the separatrix. From sequences of X-ray images, we find (in agreement with a study of other extended loops by Porter et al. 1998) that the brightness of any one of these extended loops evolves much more gradually than the brightness fluctuations (microflares) seen in the core fields at its foot, and often shows little or no response to longer-term brightness changes there. The three-dimensional topology of the magnetic field rooted in and around the island leads us to note that the basic reason that the heating of these extended loops is largely independent of the heating in the core fields may be that the magnetic null is directly involved in the heating of the extended loops but not in the heating in the core fields.

2. INSPECTION OF TWO COMPLEMENTARY ACTIVE REGIONS

Inspection of the vector magnetograms of the two active regions (Figs. 1 and 2) shows that each active region is primarily bipolar, and that each has an island of included polarity in the trailing polarity. Each island is small compared to the overall bipole, in terms of both flux and area. So the island does not destroy the overall bipolar configuration. Of course, an island does completely change the field configuration in its neighborhood. In the absence of the island, all of the trailing polarity flux in that neighborhood would connect to the leading polarity flux ahead of the main neutral line. In the presence of the island, we expect that trailing polarity flux near the island, equal in total amount to the island's flux, connects to the island in short loops, forming a closed core field enveloping the neutral line around the island, as sketched in Figure 3. There is a magnetic null over the island and a separatrix surface surrounds and encloses the island. Our two active regions are also similar in that the core field around the island is strongly sheared in each case.

The main difference seen in the vector magnetograms of our two active regions is that the core field encasing the main neutral line is much more sheared in the second active region than in the first. So we expect the coronal field arch of the envelope of the overall bipole to be more globally nonpotential in the second active region than in the first active region.

In either active region, when we compare the coronal X-ray image to the magnetogram (Figs. 1 and 2), we see that only a fraction of the area over the strong-field portions (>150 G) of the active region has strong heating (i.e., has X-ray brightness above our threshold of 1000 DN s^{-1} pixel^{-1}). Thus, only a fraction of the strong-field magnetic loops are strongly heated: something selects a subset of field lines for this strong heating.

In each active region, bright coronal loops extend away from the island of included polarity. In the first active region, loop A extends from near the island of included polarity over to the leading polarity. Thus loop A is composed of magnetic field lines that bridge the main neutral

Neutral Line
Positive Magnetic Contours
Negative Magnetic Contours
Separatrix
Separatrix Intersection with the Photosphere
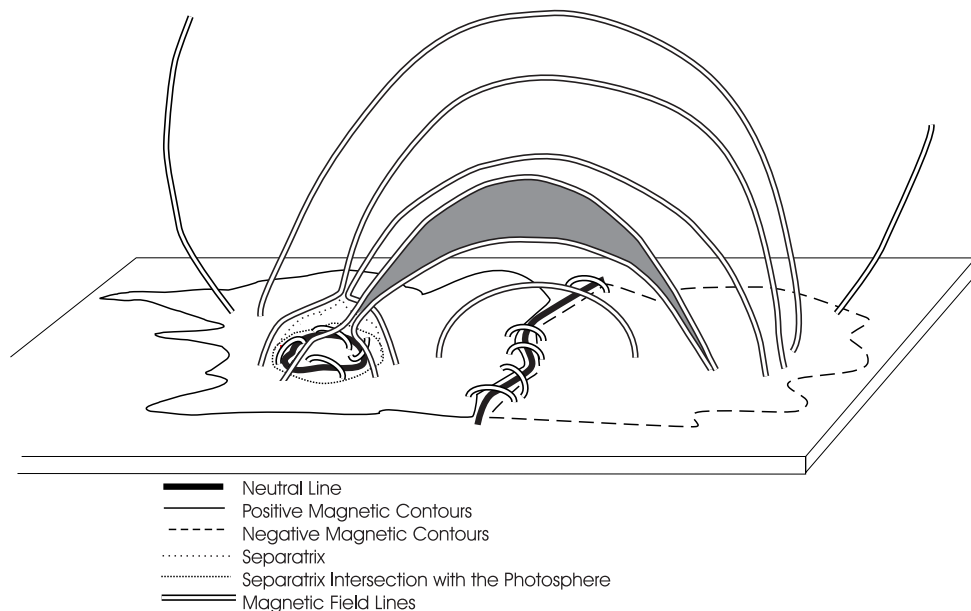Magnetic Field Lines

FIG. 3.—Illustration of the inferred magnetic field topology of our two active regions, with regard to the magnetic island and the bright extended loops of the envelope arch. The field rooted in the island of included polarity is enclosed under a separatrix surface on which there is a magnetic null above the island. The shaded extended loop is one that is strongly heated. The majority of the envelope loops, those rooted far from the island, are not strongly heated. Note that the loops rooted closely around the island in the manner of the bright loop here are in close contact with the separatrix and null, so that reconnection at the null might be essential to the selection and heating of the bright loops.

line and have their trailing footpoints rooted near but outside the island of included polarity. To the north of loop A is a bright region which was called a forest of loops in Falconer et al. (1997). This area has three bright subparts, which are labeled. Two of these loop clusters, B and C, are similar to loop A in that they connect the leading and trailing polarity regions and have their trailing polarity footpoints near the island of included polarity. Loop D is different in that it links the negative polarity island to the positive (trailing) polarity north of the island. Whereas loop D resides entirely inside the island's separatrix dome, loops A, B, and C are all entirely outside the separatrix. Also, since loop D overlies and is rooted in markedly non-potential magnetic field (see Fig. 1), it should be markedly globally nonpotential. Because the part of the active region spanned by loops A, B, and C is seen in the vector magneto-gram (Fig. 1) to be mostly more nearly potential than the part spanned by loop D, we expect loops A, B, and C to have much less global nonpotentiality than loop D. That loop C is much brighter than loops A and B and somewhat brighter than loop D suggests that an extended loop's global nonpotentiality is not the main determinant of its heating and coronal brightness.

The second active region has two extended bright loops (E and F) stemming from around the island of included polarity, and also has strong coronal heating in the sheared core field of the main neutral line. Loops E and F are similar to loops A, B, and C in that they connect the leading and trailing polarity, and their trailing polarity footpoints are rooted near an island of included polarity. Since loops E and F cross a neutral line with extensive strong magnetic shear, we expect loops E and F to be more globally non-potential than loops A, B, and C. However, from visual inspection alone there is no way to be sure of this. Also, there is no way to know from visual inspection alone if loops A, B, C, E, and F are rooted on one side of their island or straddle the island. Finally, note that since the coronal X-ray images in Figures 1 and 2 have the same brightness scale, these images show that loop C is brighter than loops E and F. This again suggests that the global nonpotentiality of an extended loop is not the main determinant of its heating and coronal brightness.

In summary, from direct inspection of the vector magne-tograms and coronal images of our two active regions, we expect that (1) both the extended loop C in the first active region and extended loops E and F in the second active region have a similar connection to the magnetic island and the sheared core field around the island and (2) loop C has little global nonpotentiality, whereas loops E and F have much global nonpotentiality. Because loop C is apparently more strongly heated than loops E and F, these two infer-ences suggest that neutral-line magnetic shear at the foot of a bright extended coronal loop dominates over the loop's global nonpotentiality in causing the strong coronal heating in the loop. This conclusion rests on the certainty of the two inferences. To certify these inferences, in the next two sections we compare the observed extended bright loops with potential magnetic loops computed from the magnetograms of the two active regions. These compari-sons (1) verify the weak global nonpotentiality of the first active region and the strong global nonpotentiality of the second active region, (2) demonstrate that the strongly heated coronal loops in each active region comprise only a small part of the overall magnetic arch rooted in the strong

field in and near the sunspots, (3) demonstrate the presence of a magnetic null over each island, and (4) indicate that for each bright extended loop that is a member of the overall magnetic arch, the foot at the island is bifurcated, so that it straddles the separatrix and embraces the null over the island in the manner sketched in Figure 3.

3. COMPARISON OF THE STRONGLY HEATED LOOPS WITH POTENTIAL FIELD LINES

In the previous section, from inspection of the vector magnetograms, neutral-line magnetic shear maps, and coronal images of our two active regions, we have inferred that (1) the first active region is globally nearly potential and the second active region is globally quite nonpotential, and (2), in either active region, only a small fraction of the volume of the magnetic arch rooted in strong field is strong-ly heated. In this section, we verify these two inferences by comparing the observed bright loops of the main arch in each active region with the three-dimensional potential field computed for that active region.

We used the Sakurai code to compute the potential field (Sakurai 1982). From the line-of-sight component of the field over the entire magnetogram, the code calculates the potential field line extending from any selected footpoint. The code takes into account the heliographic location and projects the magnetogram onto the spherical Sun. The pro-cedure ignores any observed magnetic flux outside the field of view of the vector magnetogram. This is a good approx-imation for field lines rooted in strong-field areas in an isolated active region fully covered by the magnetogram, as is the case for each of our active regions. In each active region, a fine grid of footpoints over the strong-field areas is used. We defined the strong-field area to be all magneteog-ram pixels having total measured vector magnetic field strength greater than 150 G. We chose this threshold because it includes the roots of all the bright coronal loops in our two active regions and because Falconer et al. (1997) found in a sample of about a hundred bright loops in five active regions that all were rooted in fields stronger than 150 G. In Figure 4, from the hundreds of computed field lines, we selected a subset that has enough field lines to show the overall shape and extent of the strong-field arch but is sparse enough for individual field lines to be traced by eye.

In Figure 5, computed potential field lines for the first active region are superposed on the X-ray image and neutral-line magnetic shear map for that region. The bright coronal loops A, B, and C of the main arch are fairly well aligned with the potential field, confirming our expectation from Figure 1 that this active region is globally nearly potential. These potential field lines do not fit any of loops A, B, and C perfectly, but they fit these loops much better than they fit loop D. Unlike loop D, whose negative end is in the nearby negative island, the computed potential field rooted at the positive-polarity end of loop D connects across the main neutral line to the leading negative-polarity domain of the bipole. This confirms our inference from Figure 1 that loop D is globally very nonpotential. The superposition of the potential field, neutral-line shear map, and X-ray image for our second active region is shown in Figure 6. In contrast to the first active region, loops E and F of the main arch in the second active region do not closely follow the sweep of the potential field lines. Instead, they cross the potential field lines of the main arch at large
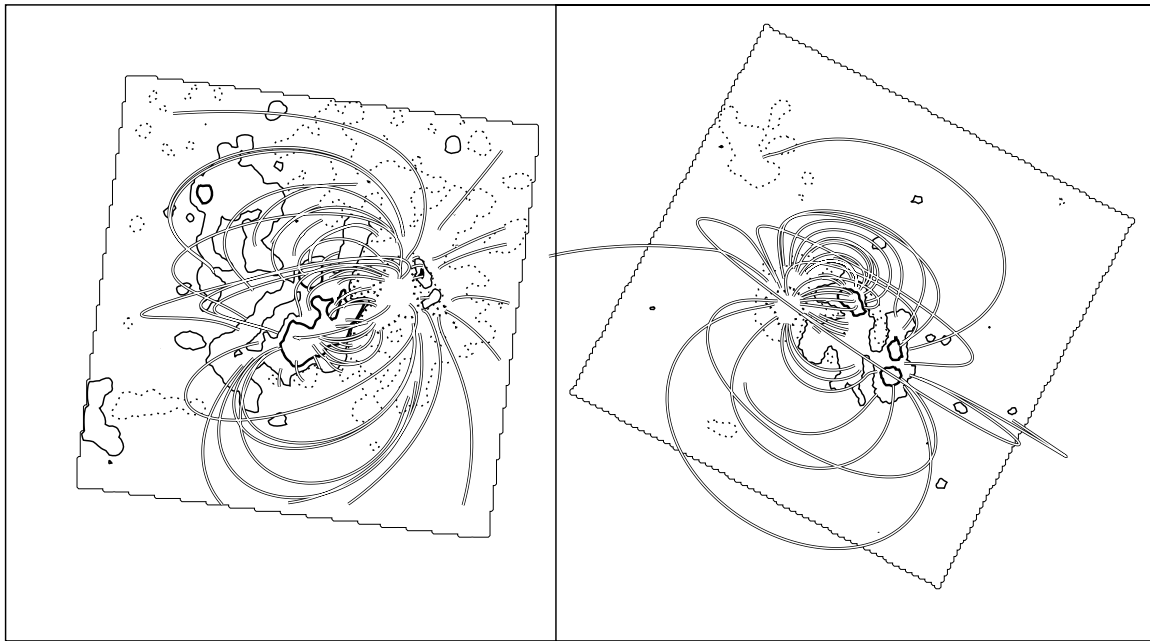
FIG. 4.—The three-dimensional potential magnetic field for each of our two active regions. *Left*: The active region of Fig. 1. The tilted square is the full field of view of the vector magnetogram, tilted so that solar north is up and west is to the right. The field lines displayed here are a subset (1:30) of those computed, each rooted in a pixel in the strong field parts of the active region (vector field strength ≤150 G). *Right*: The active region of Fig. 2. The magnetogram is displayed in the same way as in the left panel. The displayed field lines are again rooted in a subset (1:46) of the strong-field pixels.
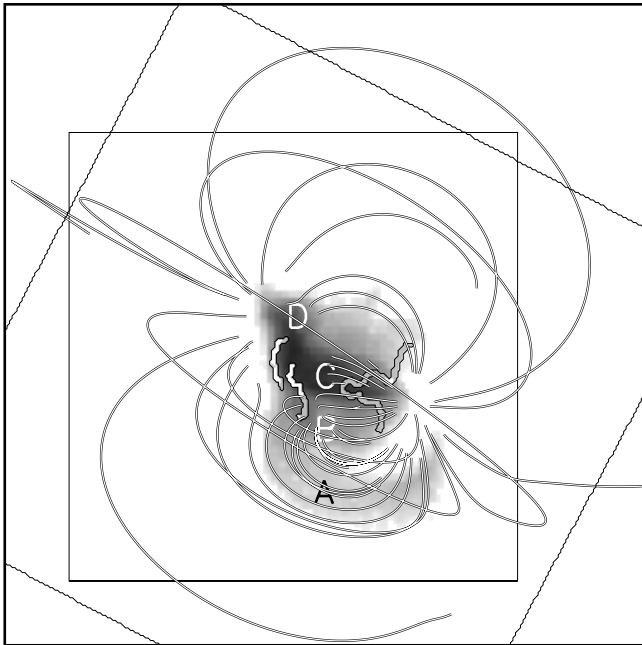

FIG. 5.—Comparison of the observed bright extended loops with the computed three-dimensional potential field in the first active region. The coronal image and neutral-line magnetic shear map are the same as in Fig. 1; the potential field lines are those shown for this active region in Fig. 4. The untilted square is the field of view of the coronal image; the tilted square is the field of view of the magnetogram. Loops A, B, and C match the direction and sweep of the potential field lines rooted near them, but loop D does not. This confirms our expectation from the vector magnetogram that the coronal arch of the overall bipole is globally nearly potential, even though the field in and around the magnetic island is grossly nonpotential.
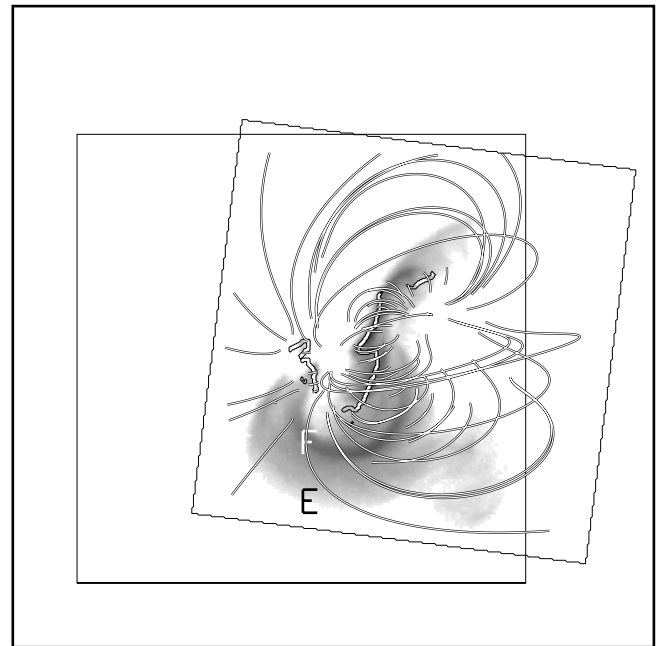

FIG. 6.—Comparison of the observed bright extended loops with the computed three-dimensional potential field in the second active region. The coronal image and neutral-line shear map are the same as in Fig. 2; the potential field lines are those shown for this active region in Fig. 4. The layout is the same as in Fig. 5. It is seen that the direction and sweep of extended loops E and F differ greatly from that of the potential field rooted near them. This confirms our expectation from the vector magnetogram that the coronal arch of the whole bipole has a large overall twist or shear of the same sense as the shear in the core field along the main neutral line.

angles, as large as the angles between the bright coronal strands of the strongly sheared core field and the potential core field along the main neutral line. This large disparity of loops E and F with the potential field shows that these loops are globally strongly nonpotential and indicates that the entire global magnetic arch of this active region is markedly nonpotential. Thus, Figure 6 confirms our expectation from Figure 2 that this active region is globally much more nonpotential than the other active region.

Figures 5 and 6 together show that even though extended loop C in the first active region is globally much less nonpotential than extended loops E and F in the second active region, loop C is much brighter than loops E and F. From this, and because all of the main-arch bright extended loops in either active region are rooted closely around an island of included polarity, we conclude that the enhanced coronal heating in bright extended loops is not set by their global nonpotentiality but by conditions at their feet. Figures 5 and 6 further support this conclusion by showing that in either active region most of the strong-field arch is rooted farther away from the island than are the bright loops of the arch, and that these much less strongly heated (much dimmer) loops fill the bulk of the volume of the whole arch. The potential magnetic field lines drawn in Figure 5 should well represent the actual strong-field coronal arch because this active region is globally nearly potential. The potential field in Figure 6 does not show the true coronal magnetic arch because this active region is globally strongly nonpotential. But, because the actual sheared global arch should have a larger volume than the potential arch (e.g., Sturrock, Antiochos, & Roumeliotis 1995) and the potential arch is rooted in the same strong-field area, the potential field does show that only a small fraction of the total volume of the actual magnetic arch is strongly heated. Thus, Figures 5 and 6 show that strong global nonpotentiality is neither a necessary nor a sufficient condition for the strong coronal heating in the bright loops of the global arch; the figures also illustrate the finding of Falconer et al. (1997) that rooting in strong magnetic field (>150 G) is a necessary but not sufficient condition for strong coronal heating in extended loops in active regions.

4. LINKAGE OF THE MAIN-ARCH BRIGHT LOOPS TO THE MAGNETIC NULL OVER THE ISLAND

As we have seen from Figures 5 and 6, the enhanced coronal heating in the main-arch bright coronal loops in our two active regions apparently arises not from the global nonpotentiality of these loops but from their having one end rooted near an island of included polarity. Hence, it seems likely that the heating is related to the structure of the magnetic field in the feet of these loops around the island. In this section we examine the three-dimensional field structure by means of the computed potential field. In the globally nearly potential active region, we suppose that those potential field lines that are rooted near the island and approximate the main-arch bright loops also embody the rudiments of the actual magnetic structure at the feet of these loops, even though the actual field at the feet is strongly nonpotential. This procedure for finding the magnetic foot structure of a main-arch bright loop cannot be directly applied in the globally strongly nonpotential active region, because there, none of the potential field lines rooted around the island even roughly fit the observed extended bright loops. However, from the similarity of the magnetic

settings of the main-arch bright loops in the two active regions, we expect that these loops all have rather similar magnetic foot structure at the island. Hence, what we can learn of this structure in the globally nearly potential active region probably holds for the other active region as well.

For the globally nearly potential active region, Figure 7 shows bundles of potential field lines that we selected for their fit to the main-arch bright loops A, B, and C. Again, the fit is not perfect, but these field lines give the best fit among the potential field lines rooted near the island. It is seen that over the island the end of each of these bundles bifurcates, so that the bundle is rooted just outside of the island, part on one side of the island and the rest on the other side. That is, the ends of these potential field bundles embrace the magnetic null and separatrix capping the island as drawn in Figure 3. Because these bundles of potential field lines fit loops A, B, and C better than other computed potential field lines do (Fig. 5), we infer that the magnetic island is embedded in the actual field in these loops in the same way as in these computed potential field lines. It is also seen in Figure 7 that between loops A and B there is a gap in which the main arch is not as strongly heated as in loops A and B. In Figure 8, the dashed potential field lines show that in this gap there is a main-arch loop that embraces the magnetic island in its split end in the same way as do loops A and B. So it appears from Figures 7 and 8 that a necessary but not sufficient condition for
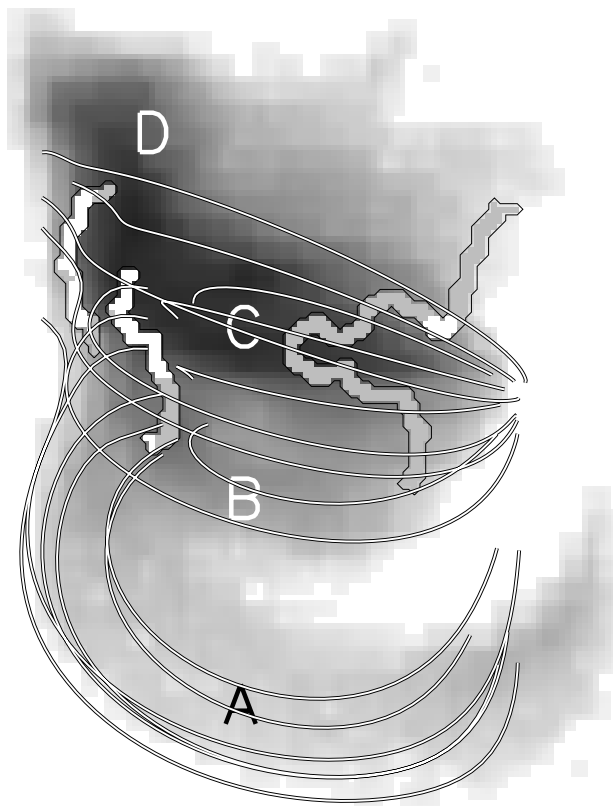

FIG. 7.—Potential field lines that trace observed bright extended loops in our globally nearly potential active region. These potential field lines were selected by their fit to loops A, B, and C in the global magnetic arch of this active region. It is seen that each of these loops is fitted by a bundle of potential field lines that straddles the magnetic island and hence has a magnetic null in its base over the island, as in the extended loops depicted in Fig. 3.
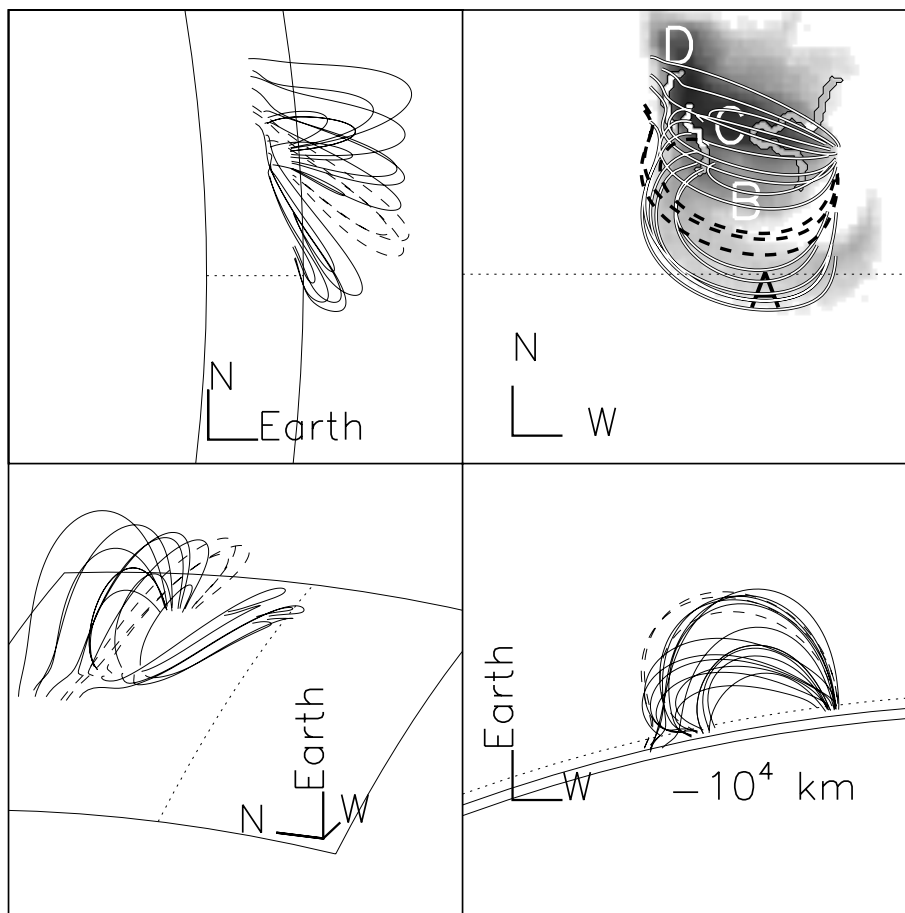
FIG. 8.—Display of the three-dimensional form of the potential field lines that fit the bright loops in the coronal arch of the globally nearly potential active region. *Upper right*: Top view from direction of Earth and *Yohkoh*. The X-ray image and the solid field lines are the same as in Fig. 7. The dashed field lines trace a magnetic loop that is sandwiched between loops A and B and that bifurcates around the magnetic island as do the feet of A and B, but that is heated much less than A and B. *Upper left*: End view from the east, showing that the plane of loop A is more nearly horizontal than vertical. *Lower right*: Side view from the south. *Lower left*: Elevated view from the southeast. In each view, the dotted line is the heligraphic equator, and the solid lines on the surface mark the edges of the field of view of the upper right panel.

strong coronal heating in a loop of the main arch is that the loop have the magnetic null of the island embedded in its foot. That is, it appears that the strong heating in a main-arch bright loop is driven from its end at the island, and that the presence of the null in the foot is necessary for the heating process to happen, but that the presence of the null does not require that the heating process be driven.

In contrast to loops A, B, and C, loop D is not a member of the main arch, is rooted in the island rather than just outside, and is topologically banned from having the magnetic null inside it. With respect to the separatrix and null over the island, loop D has the same topology as the core field encasing the neutral line around the island, and may be considered the largest of the core-field loops. Because the null is inside loops A, B, and C, but outside loop D and the rest of the core field, the null can be directly involved in the heating of loops A, B, and C but cannot be directly involved in the heating in loop D or in any other part of the core field. This suggests that the heating process in the core field and loop D is different from that in the main-arch bright loops, and raises the possibility that the two processes could be driven more or less independently, so that strong heating could occur in a main-arch loop without strong heating occurring in the core field at its foot and vice versa. In the next section we present evidence that this is indeed the case.

5. ERRATIC COUPLING OF THE HEATING IN THE MAIN-ARCH LOOPS AND THE HEATING IN THE IMPACTED CORE FIELDS

In this section we show that the heating in the main-arch bright loops proceeds independently of the heating in the core fields. This is in accord with the topological difference between the main-arch loops, which embrace the magnetic null above the island, and the island core fields, which do not.

For our globally nearly potential active region, Figure 9 compares the persistent coronal brightness image (*right panel*) examined in previous figures with corresponding images from one orbit before (*middle panel*) and three orbits before (*left panel*). In the earliest orbit (*left panel*) there is strong coronal heating in the core fields in the southern end of the island (the arrow in the left panel points to this bright core feature), at the feet of main-arch loops A and B, but A and B are not bright enough to be seen. Two orbits later (*middle panel*), the heating in the southern end of the island is much weaker, but loop B and parts of loop A have brightened above threshold. In the next orbit (*right panel*), loop B continues to be as bright as in the previous orbit, and loop A has brightened further, while the heating in the core field at their feet remains much weaker than in the first orbit. On
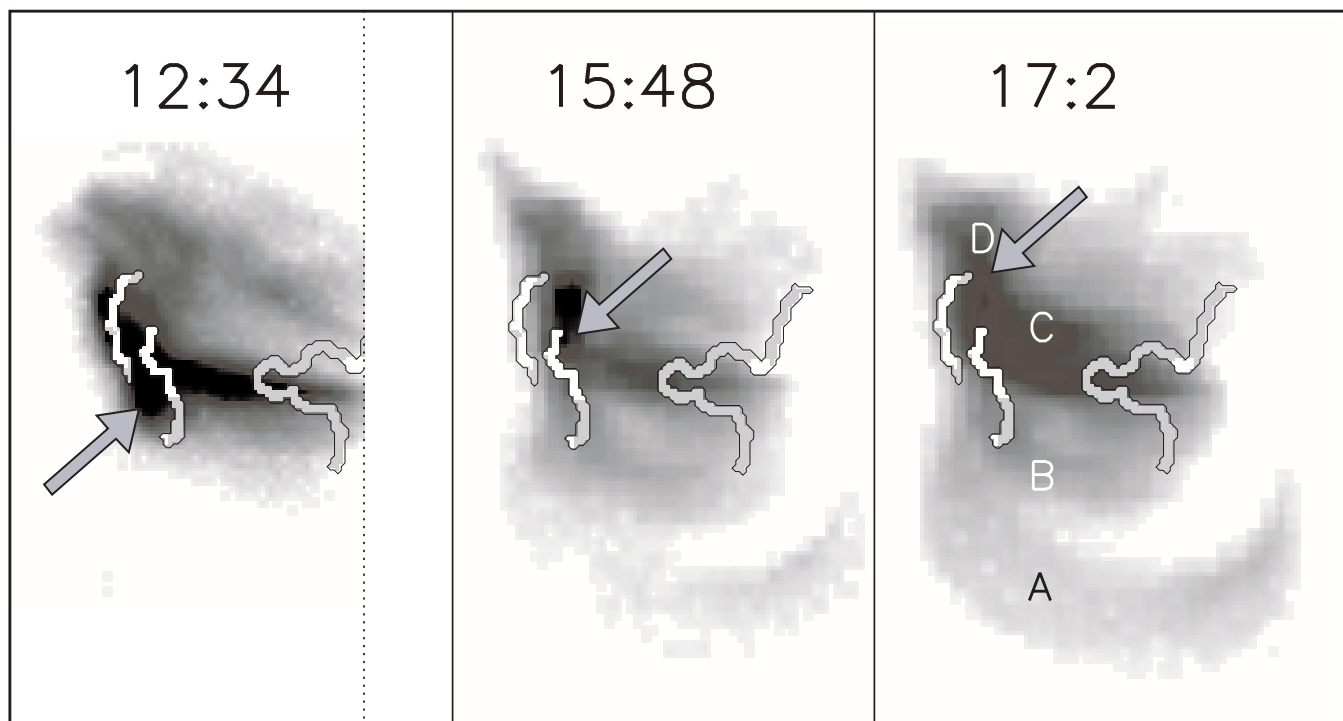
Fig. 9.—Gradual evolution of the strong coronal heating in the globally nearly potential active region over 5 hours. Each panel shows a persistent-brightness coronal X-ray image superposed on the neutral-line shear map. All three panels have the same X-ray brightness scale. The time at the top of each panel is the UT time of sunrise for the orbit of the X-ray image. The heating in all three orbits is similar in that all of the strongly heated loops are rooted in and around the magnetic island. It is also seen that extended loops A and B brighten hours after the brightness in the core fields at their feet has greatly dimmed. The arrows point to parts of the core features discussed in the text.

the other hand, main-arch loop C wanes and waxes in width and brightness in step with the persistent brightness of the core field in the middle and northern parts of the island, i.e., the core field that is impacted in the foot of loop C (the arrow in the middle panel points to this part of the bright core feature). Thus, Figure 9 shows that on orbit-to-orbit timescales there is no consistent correspondence between the level of enhanced coronal heating in the main-arch loops and that in the core fields at their feet. Figure 9 also shows that loop D, which is not a main-arch loop but an extension of the core field rooted in the northern end of the island, wanes and waxes in width and brightness along with the bright core feature at its foot (the arrow in the right panel points to this part of the bright core feature).

Figure 10 shows a steadfast difference between the heating in the main-arch loops and the heating in the core fields in and around the island: on timescales from a few minutes to an hour the main-arch loops evolve in brightness much more gradually than do the core fields and show little immediate response to sudden brightenings in the core field. In Figure 10, loops A and C gradually brighten over the orbit, while the core field undergoes two episodes of major brightening and dimming. (The core features at the island ends of loops C and D are noticeably brighter and larger in frames 2–5 and 10–12 than in the other frames.) Loop B is slightly brighter in the middle of the sequence (*middle row*) than earlier (*top row*) or later (*bottom row*) in the orbit, and shows only a slight response to the sudden localized core-field brightening at its foot (this core feature peaks in brightness in frame 5). In contrast to the main-arch loops, loop D brightens and dims and changes in substructure much more in step with the core-field brightening and dimming at its

foot in the northern end of the island. (Loop D peaks in brightness and width in frames 4 and 10.) Thus, Figures 9 and 10 both indicate that the heating process is different in the main-arch bright loops than in the core fields of the island, and that the two processes are only loosely coupled at most.

Porter et al. (1998), from a study of several other extended loops stemming from around islands of included polarity (including the island in our second active region), found a similar lack of coupling between the heating in the extended loops and the heating in the island core fields.

6. SUMMARY AND DISCUSSION

In this paper we have focused on magnetic conditions that result in the strong heating in bright coronal loops that are members of the overall magnetic arch of bipolar active regions. We have examined these conditions by comparing two complementary active regions (one globally nearly potential and the other globally strongly nonpotential), and by analyzing the magnetic structure of the bright coronal features in each active region by combining coronal X-ray images with a vector magnetogram and its neutral-line shear map and the computed potential field. We found the following:

1. The main-arch bright loops filled only a small fraction of the entire strong-field arch of each active region.

2. The main-arch bright loops were not selected for strong coronal heating on the basis of global non-potentiality.

3. Each of the main-arch bright loops in our two active regions was rooted around an island of included opposite
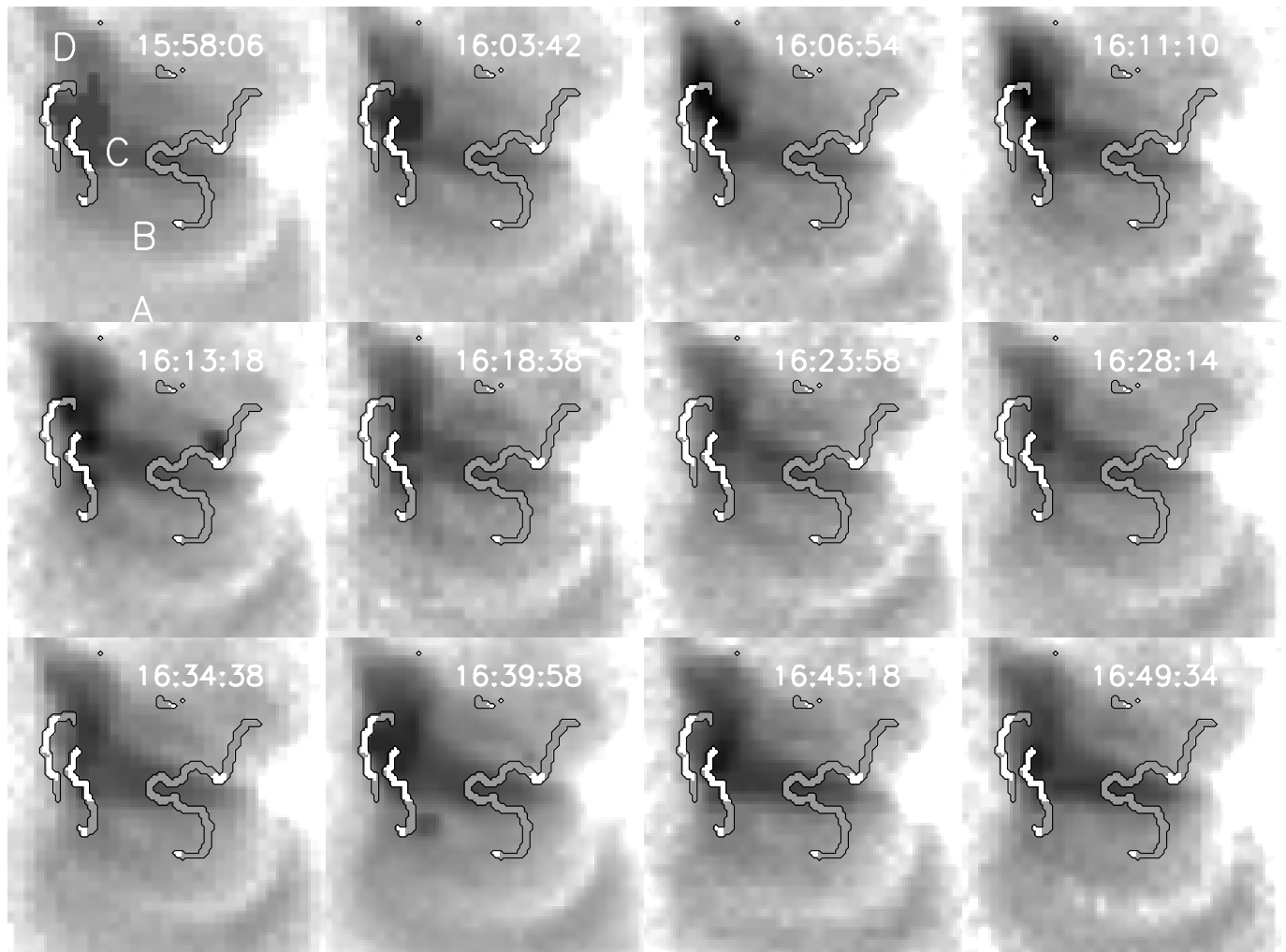
FIG. 10.—Core-field microflares and extended-loop brightness evolution during the orbit of the second panel of Fig. 9. Except for loop D, the extended loops brighten and dim more gradually than the core-field microflares, and show little immediate response to individual microflares at their feet.

polarity that had much of its neutral line encased in strongly sheared core field.

4. The end of each main-arch bright loop was probably split over the island, so that the magnetic null and separatrix over the island were embraced by the foot of the loop.

5. Not all of the main-arch loops with split ends that embraced the island and its null were selected for strong heating at the same time.

6. The strong coronal heating in the main-arch loops evolved much more gradually and largely independently of the strong coronal heating in the core fields at the feet of these bright loops.

7. The strong coronal heating in the extended loop D mimicked and tracked the rapidly changing (microflaring) strong coronal heating in the island core field at its foot.

We interpret the above results as follows:

1. There are (at least) two basically different kinds of bright extended coronal loops that have one end rooted close to a neutral line having a strongly sheared core field. The difference is in the topology of the magnetic field in the foot near this neutral line. In one kind of extended loop, the neutral line crossed by the loop is the neutral line near the end of the loop. An example of this is loop D. For this kind of extended loop, there is no requirement that the neutral line encircle an island of included polarity. With respect to the neutral line, the topology of this type of extended loop is the same as that of the core field. In the other kind of extended loop, the neutral line crossed by the loop is far from the ends of the loop. In our two active regions, this neutral line is the main neutral line of the overall bipole, and the loops of this kind are the main-arch bright loops. For this kind of extended loop, the neutral line near the end of the loop encircles an island of included polarity (of the same polarity as the far end of the extended loop), and the loop is rooted on both sides of the island in the surrounding opposite polarity flux, so that the island and the magnetic null and separatrix over the island are straddled by the split end of the loop.

2. In either kind of extended bright coronal loop, the heating is driven from the end near the neutral line and sheared core field, but the heating process is different for the two kinds of loops. In the kind that crosses its end neutral line, there is no permanent magnetic separatrix and null directly involved in the heating. Instead, the heating is similar to, and/or coupled to, the microflare-like heating in the sheared core field. In the other kind of extended loop,

with an end embracing an island of included polarity, the permanent magnetic null over the island and in the split end of the loop is directly involved in the heating. A likely possibility is that reconnection is driven at the null and the heating in the loop is a product of this reconnection process. Such reconnection at the null over a magnetic island has been modeled by Yokoyama and Shibata (1996) and by Karpen, Antiochos, & DeVore (1996) and shown to be a promising mechanism for heating extended loops of this kind. The reconnection might be driven by emerging magnetic flux as modeled by Yokoyama & Shibata (1996), or by shearing of the magnetic field across the separatrix by photospheric flows as modeled by Karpen et al. (1996), or by eruptive action of the sheared core field triggered by flux cancellation at the neutral line as Moore et al. (1999) have suggested for driving and heating in the extended loops and for driving the heating in the sheared core fields. Why the heating in these extended loops is only loosely coupled to the heating in the core fields at their feet is a basic question raised but not answered by our results and the similar results of Porter et al. (1998). To answer this question may require long sequences of vector magnetograms having sub-arcsecond resolution together with coronal images with similar resolution. Such observations are expected from the Japan/US/UK *Solar-B Mission* now planned for launch in 2004.

REFERENCES

Falconer, D. A., Moore, R. L., Porter, J. G., Gary, G. A., & Shimizu, T. 1997, ApJ, 482, 519
Karpen, J. T., Antiochos, S. K., & DeVore, C. R. 1996, ApJ, 460, L73
Moore, R. L., Falconer, D. A., Porter, J. G., & Suess, S. T. 1999, ApJ, 526, 505
Moore, R., Porter, J., Roumeliotis, G., Shimizu, T., Tsuenta, S., Sturrock, P. A., & Acton, L. W. 1994, in Proc. Kofu Symp. New Look at the Sun ed. S. Enome & T. Hirayam (Nobeyama Radio Obs. Rep. 360; Nagano: Nobeyama Radio Observatory), 89
Porter, J. G., Falconer, D. A., & Moore, R. L. 1998, in Solar Jets and Coronal Plumes, ed. T.-D. Guyenne (ESA SP-421; Noordwijk: ESA Pub. Div., ESTEX), 147
Porter, J., Moore, R., Roumeliotis, G., Shimizu, T., Tsuenta, S., Sturrock, P. A., & Acton, L. W. 1994, in Proc. Kofu Symp., New Look at the Sun, ed. S. Enome & T. Hirayam (Nobeyama Radio Obs. Rep. 360; Nagano: Nobeyama Radio Observatory), 65
Sakaurai, T. 1982, Sol. Phys., 76, 301
Schrijver, C. J., et al. 1999, Sol. Phys., 187, 261
Sturrock, P. A., Antiochos, S. K., & Roumeliotis, G. 1995, ApJ, 443, 804
Vaiana, G. S., & Rosner, R. 1978, ARA&A, 16, 393
Yokoyama, T. & Shibata, K. 1996, PASJ, 48, 535